Rb *nf* quantum defects from millimeter-wave spectroscopy of cold ^{85}Rb Rydberg atoms

Jianing Han, Yasir Jamil,* D. V. L. Norum, Paul J. Tanner, and T. F. Gallagher
Department of Physics, University of Virginia, Charlottesville, Virginia 22904, USA
(Received 2 August 2006; published 16 November 2006)

Millimeter-wave resonance spectroscopy has been used to measure the $(n+2)d_{5/2}$ to $nf_{5/2,7/2}$ transition frequencies of cold ^{85}Rb atoms in a magneto-optical trap. From these intervals we extract substantially improved Rb *nf* quantum defects, fine structure intervals, and limits for the dipole and quadrupole polarizabilities of Rb^+.

DOI: 10.1103/PhysRevA.74.054502 PACS number(s): 32.30.Bv, 32.10.Fn, 32.80.Pj

Accurate values of the quantum defects of the high angular momentum states of alkali atoms are of interest for two reasons. First, they are important for precise calculations of the Stark effect [1,2], and second, the polarizabilities of the core can be extracted from the quantum defects of the nonpenetrating states [3,4]. Systematic measurements of the high ℓ-state quantum defects of Li, Na, and Cs have been done, but none have been done for K or Rb [4]. Here we report the measurement of the Rb *nf* quantum defects and fine-structure intervals using a millimeter (mm) wave resonance approach.

The apparatus and technique are similar to those described by Li *et al.* [5], and the essential ideas are shown in Fig. 1. Rb atoms are held in a vapor cell magneto-optical trap (MOT) [6]. The 780 nm trapping lasers establish a steady-state population of 3×10^5 atoms in the $5p_{3/2}$ state, and the MOT volume of ~1 mm^3 is midway between two pairs of rods, which serve as field-ionization electrodes. The $5p_{3/2}$ atoms are excited to the Rb $(n+2)d$ state at a 20 Hz repetition rate with a 480 nm 5 ns dye laser pulse, which populates preferentially the Rb $(n+2)d_{5/2}$ level. Subsequent to the dye laser pulse the atoms are exposed to a 5-μs-long mm wave pulse to drive the $(n+2)d_{5/2}$ to nf_j transition. The mm waves are generated by frequency multiplying the 12–20 GHz output of an Agilent 83622B synthesizer. Immediately after the mm wave pulse the atoms are exposed to a 2 μs rise time field-ionization pulse. Atoms in the *nf* state ionize at a higher field than do atoms in the $(n+2)d$ state, resulting in temporally resolved ion signals from field ionization of the $(n+2)d$ and *nf* states. The *nf* signal is recorded with a gated integrator as the mm wave frequency is swept across the atomic resonance over many shots of the laser. The sweep is repeated until an acceptable signal-to-noise ratio is obtained.

A substantial improvement over the measurements of Li *et al.* [5] is the elimination of the magnetic field. We turn off the MOT trapping magnetic field 20 ms before the laser fires. When the laser fires we estimate that the trap fields have fallen to a value less than 0.06 G. Using three sets of nulling coils we cancel the residual static magnetic fields in three orthogonal directions using a variant of the method of Afrousheh *et al.* [7]. To null the field in a particular direction we apply a field from −0.5 to 0.5 G in that direction while the other two directions have small, if any, magnetic fields. We typically observe three resonances, two of which have large, 1.6 MHz/G, frequency shifts, which are linear in the magnetic field for fields of magnitude greater than 0.15 G. The average of the nulling fields that produce the same magnitude of positive and negative frequency shift produces zero magnetic field in this direction. This process is iterated for all three directions. From the variation in the width of the observed resonance with applied field and the observed line shape in nominally zero field, especially the appearance of the subsidiary maxima [8], as shown in Fig. 2, we estimate the residual field to be less than 0.06 G.

The microwave power is reduced to the point at which power broadening is eliminated, and a typical resonance signal is shown in Fig. 2, a recording of the $32d_{5/2}-30f_{7/2}$ transition obtained with a 5-μs-long microwave pulse. It exhibits the expected two-level resonance line shape calculated for $\Delta m_j=0$ transitions for a mixture of m_j levels. The line centers may be determined within ±30 kHz from the observed resonances. The largest uncertainty comes from the Stark shifts due to residual stray fields. The Stark shifts are large due to the proximity of the *nf* and *ng* states. For example, the $35g$ state is only 2 GHz away from the $35f$ state. We are able to null the stray field in one direction by applying a small bias voltage to the field ionization rods. To find the correct

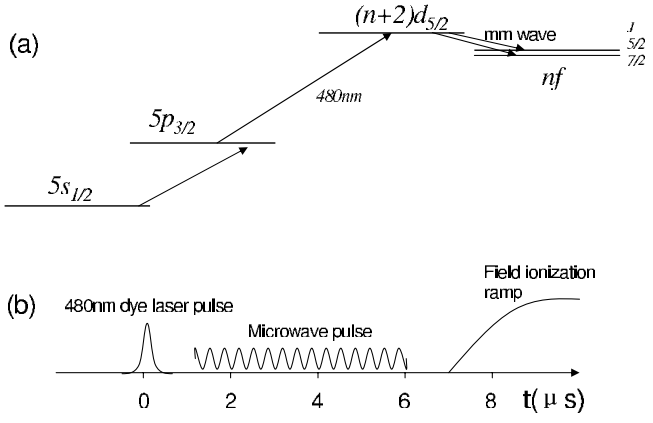

FIG. 1. (a) Energy-level diagram. The 780 nm trap laser excitation of the $5p_{3/2}$ state and the 480 nm dye laser excitation of the $(n+2)d$ state are shown by the upward arrows, and the mm wave transitions to the $nf_{5/2}$ and $nf_{7/2}$ states are shown by the downward bold arrows. (b) Timing diagram. The dye laser pulse is followed by the 5-μs-long mm wave pulse and the field-ionization ramp.

*On leave from the Department of Physics, University of Agriculture, Faisalabad and supported by the Higher Education Commission of Pakistan.

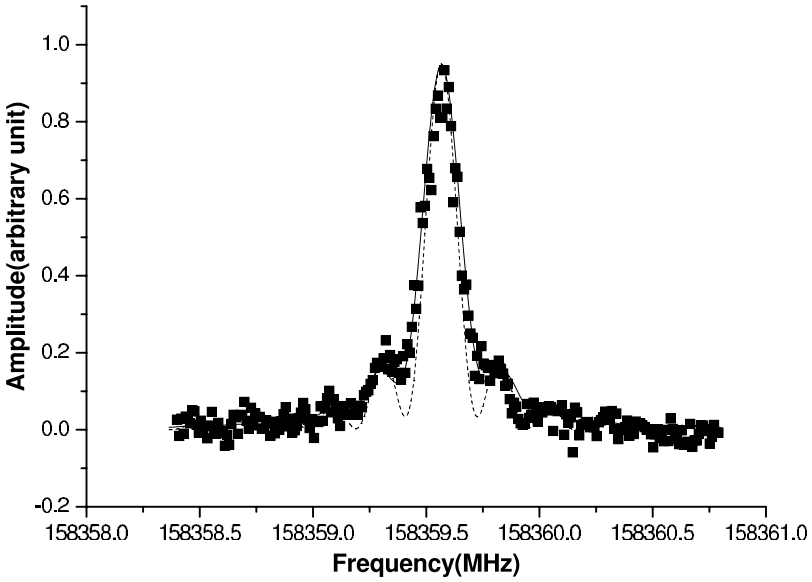

FIG. 2. The $32d_{5/2}-30f_{7/2}$ resonance observed with a 5-μs-long mm wave pulse (■). Calculated resonance assuming a 36 mG magnetic field and a 10 μV/cm microwave field amplitude (———). Calculated resonance with zero magnetic field and a 10 μV/cm microwave field amplitude (----).

bias voltage we measure the resonance frequency as a function of applied bias voltage, fit the frequency shift to a quadratic bias voltage dependence, and set the bias voltage at the minimum frequency shift. The day-to-day variation in the bias voltage required to null one component of the stray field indicates the magnitude and variation in the stray field in this direction. Assuming the stray fields in all directions to be of the same magnitude we estimate the typical residual stray field in our measurements to be 20 mV/cm. Accordingly, we present in Table I the results of our measurements and the results corrected by removing the Stark shift due to a 20 mV/cm residual field. The measurement uncertainties are increased by adding the Stark shift from a 20 mV/cm field in quadrature. Although the sensitivity of the mm wave resonance frequency to an electric field is a nuisance in this context, as shown by Osterwalder and Merkt, it can be used to measure the fields [9].

TABLE I. Observed and corrected Rb $(n+2)d_{5/2}-nf_j$ intervals.

N	Observed intervals (MHz)	Corrected intervals (MHz)
	$(n+2)d_{5/2}-nf_{5/2}$	$(n+2)d_{5/2}-nf_{5/2}$
30	158353.829(42)	158353.81(5)
31	143655.355(29)	143655.33(4)
32	130721.395(37)	130721.37(5)
33	119294.819(29)	119294.78(5)
34	109162.277(34)	109162.23(6)
35	100145.626(26)	100145.57(6)
36	92095.381(48)	92095.32(8)
37	84885.449(45)	84885.37(9)
	$(n+2)d_{5/2}-nf_{7/2}$	$(n+2)d_{5/2}-nf_{7/2}$
30	158359.549(18)	158359.53(3)
31	143660.599(14)	143660.58(3)
32	130726.182(68)	130726.15(7)
33	119299.161(14)	119299.13(4)
34	109166.271(11)	109166.23(5)
35	100149.284(28)	100149.23(6)
36	92098.727(28)	92098.66(7)
37	84888.544(42)	84888.46(9)

From the corrected intervals of Table I and the known quantum defects of the Rb $nd_{5/2}$ states [5] it is a straightforward matter to extract the nf quantum defects. Specifically, the frequency interval between the two states $n\ell_j$ and $n'\ell'_{j'}$ can be expressed by

$$\upsilon_{n'\ell'j'n\ell j} = R_{\mathrm{Rb}}c\{[n' - \delta_{\ell'j'}(n')]^{-2} - [n - \delta_{\ell j}(n)]^{-2}\}, \quad (1)$$

where n is the principal quantum number, $R_{\mathrm{Rb}}=109\,736.605\ \mathrm{cm}^{-1}$ is the Rydberg constant of rubidium, $c=2.99792458\times10^{10}$ cm/s is the speed of light, and $\delta_{\ell j}(n)$ and $\delta_{\ell' j'}(n')$ are the quantum defects of the initial and final states, which mainly depend on ℓ and slightly on n and j. For $n \geqslant 20$, the quantum defect can be expressed as [5]

$$\delta_{\ell j}(n) = \delta_{\ell j0} + \frac{\delta_{\ell j2}}{(n-\delta_{\ell j0})^2}, \quad (2)$$

where $\delta_{\ell j0}$ and $\delta_{\ell j2}$ are constants. Using the known values of $\delta_{\ell j0}$ and $\delta_{\ell j2}$ for the Rb $nd_{5/2}$ states we obtain quantum defects, which are substantially improved over the previous values [10,11], as shown in Table II.

The difference in the frequencies of the transitions to the $nf_{5/2}$ and $nf_{7/2}$ states is the fine structure interval of the nf state. Previously, only the $6f$ and $7f$ fine-structure intervals

TABLE II. The previous and improved quantum defect constants for the nf series.

		Previous value	Improved value
$nf_{5/2}$	δ_0	0.016312	0.0165192(9)
	δ_2	−0.064007	−0.085(9)
$nf_{7/2}$	δ_0	0.016312	0.0165437(7)
	δ_1	−0.064007	−0.086(7)

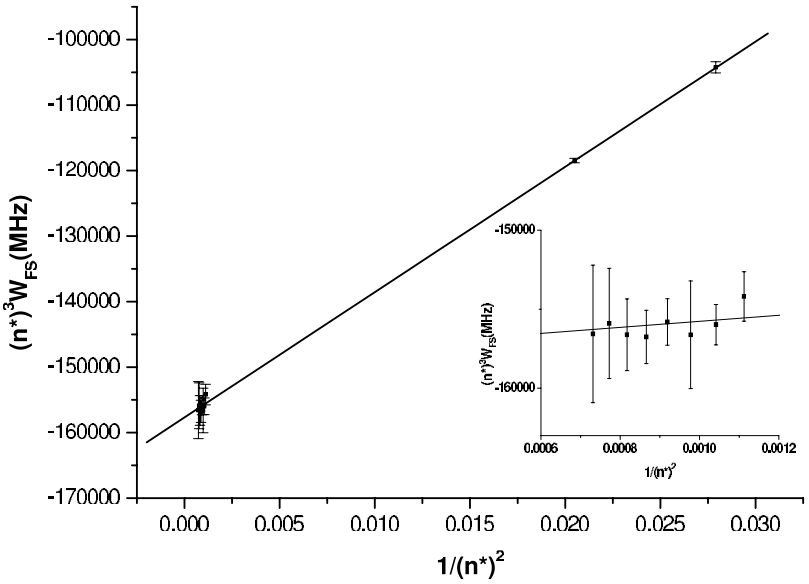

FIG. 3. The n^{*3} scaled fine-structure intervals of the Rb nf state vs $1/n^{*2}$. The two low n points are from Ref. [12].

had been measured [12], and our measurements allow a determination of the asymptotic high-n dependence. The interval is inverted for all n, and in Fig. 3 we plot the scaled fine-structure interval $n^{*3}W_{FS}$ vs $1/n^{*2}$, where n^* is the effective quantum number of the center of gravity of the nf state. The fine-structure intervals can be fit to the form

$$W_{FS} = \frac{A}{n^{*3}} + \frac{B}{n^{*5}}, \tag{3}$$

where A and B are constants. Fitting to this function yields the fine-structure constants: $A=-157.68(25)$ GHz, $B=1.917(13)$ THz. The previous values for these two constants are $A=-152$ GHz and $B=1.82$ THz [4]. For comparison, the hydrogenic nf fine structure is fit by Eq. (3) using $A=14.61$ GHz and $B=0$.

The inverted fine structure indicates that the Rb nf states are the highest ℓ states that exhibit core penetration [4]. Consequently, measurements of $\ell \geqslant 4$ states will be required to determine the Rb^+ core polarizabilities precisely. However, with these nf quantum defects and a preliminary value of the ng quantum defect, 0.00400(9), which we have obtained from microwave two-photon $(n+2)d-ng$ measurements, we can place limits on the Rb^+ polarizabilities. Recently, Afrousheh *et al.* have reported a value of 0.00405(6) for the Rb ng quantum defect using a very different technique [13]. Using the core-polarization model, i.e., assuming no core penetration, we can express the quantum defect of the center of gravity of the $n\ell$ state as

$$\delta_{n\ell} n^{-3} = \frac{\alpha_d}{2}\langle r_{n\ell}^{-4}\rangle + \frac{\alpha_q}{2}\langle r_{n\ell}^{-6}\rangle, \tag{4}$$

where α_d and α_q are the dipole and quadrupole polarizabilities of the ion core. If we rewrite Eq. (4) as

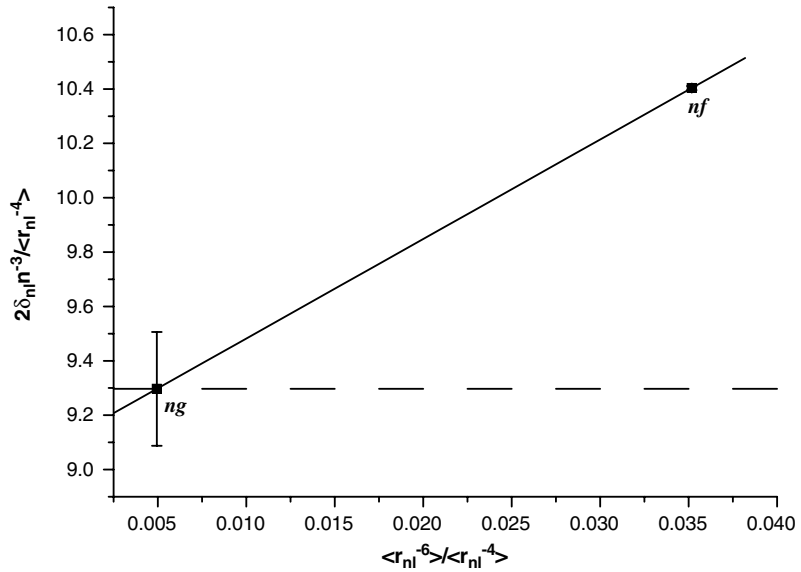

FIG. 4. Plot of the left-hand side of Eq. (8) vs $\langle r_{n\ell}^{-6}\rangle/\langle r_{n\ell}^{-4}\rangle$. Assuming there to be no core penetration in the nf states leads to the solid line with slope and intercept α_q and α_d, the quadrupole and dipole polarizabilities of Rb^+. Assuming that the nf quantum defect is larger than the ng quantum defect only because of core polarization leads to an upper limit to α_d shown by the broken line.

$$\frac{2\delta_{n\ell}n^{-3}}{\langle r_{n\ell}^{-4}\rangle} = \alpha_d + \frac{\alpha_q\langle r_{n\ell}^{-6}\rangle}{\langle r_{n\ell}^{-4}\rangle}, \tag{5}$$

and plot the left-hand side of Eq. (5) vs $\langle r_{n\ell}^{-6}\rangle/\langle r_{n\ell}^{-4}\rangle$ we obtain the polarization graph shown in Fig. 4. The nf point lies higher than the ng point because of the contributions of α_q and core penetration, both of which are positive. If there were no penetration in the nf states the intercept and slope would give $\alpha_d=8.9a_0^3$ and $\alpha_q=43a_0^5$, which are the lower and upper limits of α_d and α_q, respectively. On the other hand, assuming that the nf point lies above the ng point only because of penetration leads to $\alpha_d=9.3a_0^3$ and $\alpha_q=0$. In sum $8.9a_0^3<\alpha_d<9.3a_0^3$ and $0<\alpha_q<43a_0^5$. The calculated values of α_d and α_q are $10.22a_0^3$ [14] and $38.43a_0^5$ [15]. While the calculated and measured values of α_q are consistent with each other, the calculated value of α_d is 10% higher than the measured value.

The measurements reported here lead to Rb nf quantum defects, which differ substantially ($>1\%$) from the previous values and are several orders of magnitude more accurate, and they show that the nf fine-structure intervals are inverted for all n. Finally, we are able to set limits on the core polarizabilities of Rb^+.

It is a pleasure to acknowledge helpful discussions with T. Bergeman, M. W. Noel, R. R. Jones, and J. D. D. Martin. We thank Xiangdong Zhang for writing the program to accumulate the data. This work has been supported by the Air Force Office of Scientific Research.

[1] G. D. Stevens, C.-H. Iu, T. Bergeman, H. J. Metcalf, I. Seipp, K. T. Taylor, and D. Delande, Phys. Rev. A **53**, 1349 (1996).
[2] T. Bergeman (private communication).
[3] B. Edlen in *Handbuch der Physik*, edited by S. Flugge (Springer-Verlag, Berlin, 1964).
[4] T. F. Gallagher, *Rydberg Atoms* (Cambridge University Press, Cambridge, 1994).
[5] W. Li, I. Mourachko, M. W. Noel, and T. F. Gallagher, Phys. Rev. A **67**, 052502 (2003).
[6] C. Monroe, W. Swann, H. Robinson, and C. Wieman, Phys. Rev. Lett. **65**, 1571 (1990).
[7] K. Afrousheh, P. Bohlouli-Zanjani, J. D. Cater, A. Mugford, and J. D. D. Martin, Phys. Rev. A **73**, 063403 (2006).
[8] N. F. Ramsey, *Molecular Beams* (Oxford University Press, New York, 1956).
[9] A. Osterwalder and F. Merkt, Phys. Rev. Lett. **82**, 1831 (1999).
[10] I. Johansson, Ark. Fys. **15**, 169 (1958).
[11] C.-J. Lorenzen and K. Niemax, Phys. Scr. **27**, 300 (1983).
[12] J. Farley and R. Gupta, Phys. Rev. A **15**, 1952 (1977).
[13] K. Afrousheh, P. Bohlouli-Zanjani, J. A. Petrus, and J. D. D. Martin, Phys. Rev. A (to be published).
[14] J. Heinrichs, J. Chem. Phys. **52**, 6316 (1970).
[15] R. M. Sternheimer, Phys. Rev. A **1**, 321 (1970).